1997. *Huygens: Science, Payload and Mission. ESA SP-1177* (A. Wilson, Ed.), pp.287-298.

# Titan Zonal Wind Model

F. M. Flasar,[1] M. D. Allison[2] & J. I. Lunine[3]

[1]*Laboratory for Extraterrestrial Physics, NASA/Goddard Space Flight Center, Greenbelt, MD 20771, USA*
*E-mail: mike@leprss.gsfc.nasa.gov Fax: +1 301 286-1683*
[2]*NASA/Goddard Institute for Space Studies, 2880 Broadway, New York, NY 10025, USA*
[3]*Lunar and Planetary Laboratory, University of Arizona, Tucson, AZ 85721, USA*

**Information on Titan's zonal winds is sparse and derives primarily from temperatures retrieved from Voyager infrared measurements and geopotential heights retrieved from ground-based observations of the 28 Sgr occultation. The inferred winds are primarily zonal (i.e., east-west) and cyclostrophic in much of the atmosphere. The direction of the winds is not constrained by the data, although plausible arguments based on the spin-up of an atmosphere from an initial motionless state suggest that the winds blow predominantly in the direction of the planetary rotation. We present a conservative envelope of the vertical and meridional structure of the zonal winds, based on the available data and theoretical considerations, and briefly describe prospects for an improved wind determination prior to the insertion of Cassini into orbit about Saturn. We also briefly discuss the effect of the uncertainty in the zonal winds on the entry of the Huygens probe.**

## 1. Introduction

Voyager 1's flyby of Titan gave the first indication that the moon's atmosphere as a whole superrotated cyclostrophically, i.e., well in excess of the surface rotation rate. This suggested that Titan's global circulation might be similar in many respects to that of Venus, where the cyclostrophic wind system has been extensively documented by both in situ and remote sensing measurements from several space missions and Earth-based observations. This realisation was particularly important because the evolution and maintenance of cyclostrophic atmospheres is not very well understood, and the prospect of having another one to study, with a solar forcing and thermal response rather different from that on Venus, has offered the prospect of further insights into these complex dynamical systems.

The inference of cyclostrophic zonal winds on Titan is based on temperature and geopotential height fields retrieved from Voyager and subsequent ground-based observations. The spatial coverage of these measurements, although they include high and low latitudes, is nonetheless sparse. More direct measurements, for example, from tracking discrete cloud features or in situ measurements, do not exist.

This paper presents the atmospheric zonal wind model that has been used in Huygens' design and in planning its release from Cassini and its descent through Titan's atmosphere. Section 2 discusses the measurements on which the wind model is based, and also theoretical considerations pertaining to the meridional structure of the wind profile and its probable direction. Section 3 summarises the vertical and meridional structure of the recommended envelope of the zonal winds for mission planning purposes. Section 4 discusses the implications of the uncertainties in the wind profile for the Probe's descent trajectory, and section 5 discusses future

observations that may provide an improved determination of Titan's winds before Cassini's arrival in the saturnian system in 2004. Of necessity, the presentation is brief. For a more complete discussion of Titan's zonal winds, including the theoretical framework, we recommend the reviews by Hunten et al. (1984) and Flasar & Conrath (1992). The latter reviews the dynamic meteorology of Titan and touches on several of the points in this paper. Hubbard et al. (1993) present the analysis of the important data set afforded by the occultation of 28 Sgr by Titan. Allison et al. (1994) discuss how the constraint of zero Ertel potential vorticity implies a meridional structure that appears to agree with the meridional profiles of the zonal winds observed on Venus and in Titan's upper stratosphere. Some of the material in this paper was included in an earlier informal 'white paper' by Lunine et al. (1991), which addressed various concerns about the Probe's descent arising from uncertainties in the zonal winds.

## 2. Measurements and Derived Winds

What little is known about Titan's winds has been inferred from temperatures retrieved from Voyager 1's infrared spectroscopy experiment (IRIS) and from the geopotential heights retrieved from the light curves recorded by various terrestrial observatories during Titan's occultation of 28 Sgr in 1989. The geopotential,

$$\phi = \int_0^z g\mathrm{d}z' \,, \tag{1}$$

is related to the zonal winds through the gradient wind equation:

$$u\left[2\Omega \sin \Lambda + u\frac{\tan \Lambda}{r}\right] = -\left(\frac{1}{r}\frac{\partial \phi}{\partial \Lambda}\right)_p \tag{2}$$

Here $g$ denotes the gravitational acceleration, $z$ is altitude, $u$ is the zonal (east-west) velocity (positive in the eastward direction), $\Omega = 2\pi/16$ days is the surface rotation rate, $\Lambda$ is the latitude, $r$ is the distance from the centre of the planet, and $p$ is pressure. The cyclostrophic limit is attained when the second term on the left-hand side dominates: $u \gg \Omega r$. (In the geostrophic limit — more familiar in the meteorology of rapid rotators such as Earth, Mars and the giant planets: $u \ll \Omega r$, and the first term on the left dominates.) By combining (2) with the barometric pressure law, we obtain the *thermal wind relation*,

$$\frac{\partial}{\partial \ln p}\left[u\left(2\Omega \sin \Lambda + \frac{u \tan \Lambda}{r}\right)\right] = \frac{R}{r}\left(\frac{\partial (T/\mu)}{\partial \Lambda}\right)_p \,, \tag{3}$$

where $T$ is temperature, $R$ is the universal gas constant, and $\mu$ is the molecular weight ($\sim 28$). The potential source of molecular weight fluctuations in (3) is methane, which is a condensible. The effect is important only in the lower troposphere. We might expect the variations of $T$ and $1/\mu$ to be positively correlated if a global ocean controlled atmospheric methane: higher temperatures should be correlated with higher vapour pressures and, in a predominantly nitrogen atmosphere, lower molecular weight. With a 95K surface temperature (Flasar et al., 1981) and maximum surface relative humidity of 70-83% (Flasar, 1983; Lellouch et al., 1989), the fractional change in $\mu$ is one-third to one-half that in $T$. In the following discussion, possible meridional variations in $\mu$ will be ignored and the resulting errors absorbed in uncertainties in $T$. Note that, in equations (2) and (3), the meridional gradients are taken along isobaric surfaces. Furthermore, the dependent variables $u$, $\phi$ and $T/\mu$ are zonal averages, i.e. they are averages around latitude circles.

### 2.1 28 Sgr

In the summer of 1989 a battery of professional and amateur astronomers in Europe, Central Asia and the Middle East observed the occultation of the bright K giant star 28 Sgr by Titan. Early analysis of the measured light curves showed a central flash, indicating that Titan's atmosphere near 0.25 mbar was not spherically symmetric but had an equatorial bulge. Although not constrained by the data, this bulge was consistent with symmetry about the planetary axis of rotation, as might be produced by zonal cyclostrophic winds blowing around this axis (Sicardy et al., 1990; Hubbard et al., 1990). Subsequent analysis of the shape of the central flash caustics (Hubbard et al., 1993) revealed that the iso-density surfaces were not simply ellipsoidal but, instead, were more flattened near the equator, as shown by the dashed curve in Fig. 1. The unshaded region in Fig. 1 denotes the latitudes of the periapses of the light rays producing the central flash. Latitudes poleward of 65° in either hemisphere were not sampled because the north pole was tilted toward Earth; the season on Titan was close to northern summer solstice. Neither did rays with periapsis latitudes north of 20°S contribute significantly to the central flash because of obscuration by the enhanced northern hemispheric haze. The iso-density height curve in Fig. 1 is the result of an 8th-order Legendre polynomial fit to the entire globe that assumed symmetry about the rotation axis and the equator. Hence only five even Legendre polynomials were retained in the fit.

The solid curve in Fig. 1 denotes the zonal winds, derived from the gradient wind equation (2) under the assumption that the iso-density and isobaric surfaces coincide at 0.25 mbar; in other words, there are no temperature gradients along these surfaces. The smaller-scale oscillations in latitude are artifacts of the series truncation. Keeping in mind the restricted latitude range sounded, we can plausibly conclude that the zonal velocity profile is reasonably flat at low latitudes, and there appears to be a jet near 60°. The dotted curve is a zonal velocity profile for which the angular momentum per mass remains constant with latitude along the 0.25 mbar isobar. It provides a reasonable envelope to the velocity profile derived from the height curve. The assumption that $(\partial T/\partial \Lambda)_{p=0.25\ mbar}=0$ is probably unrealistic, given the temperature contrasts that Voyager's IRIS observed in the upper stratosphere in 1981 (see below). When temperatures decrease poleward, the heights of isobaric surfaces decrease more rapidly with latitude than those of iso-density surfaces, implying larger winds than Fig. 1 indicates. Hubbard et al. (1993) estimated that, if the 0.25 mbar temperature

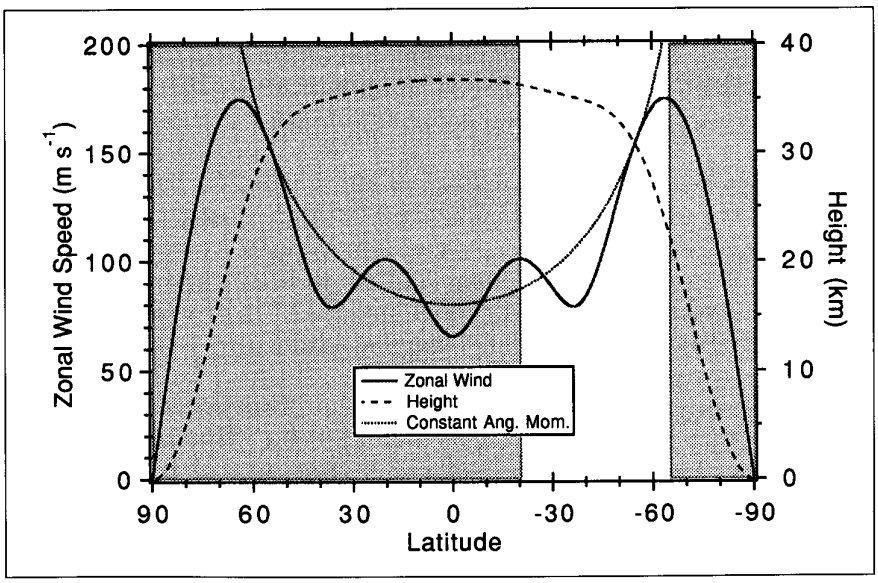


**Fig. 1. Atmospheric variables retrieved from the central flash data obtained during the 28 Sgr occultation by Titan. *Dashed curve*: height of the isodensity surface *vs* latitude. The surface is at an isobaric height of 0.25 mbar. *Solid curve*: zonal wind speeds on this surface, assuming that it is also an isobar. *Dotted curve*: wind speeds expected if the angular momentum per unit mass is constant along the isobar. The shaded regions denote periapsis latitudes not accessible to the observed central flash rays, either because of Titan's polar tilt toward Earth or because of obscuration by the global haze north of 20°S. Adapted from Hubbard et al. (1993).**

contrasts were comparable to those observed by IRIS in 1981, the implied winds would be only 15% larger than indicated in Fig. 1.

### 2.2 Voyager IRIS

The bulk of the information on the horizontal structure of temperature in Titan's atmosphere is provided by the infrared spectroscopy experiment (IRIS) on Voyager 1 in 1981, just after Titan's northern spring equinox. IRIS was not able to map Titan in the true sense of the word, but it made observations covering most latitudes within 60° N-S, with limited zonal coverage (see Fig. 1 of Flasar & Conrath, 1992). The available IRIS observations suggested that, overall, the zonal contrasts in temperature were small, certainly less than the meridional contrasts (Flasar et al., 1981). Over much of the thermal-IR spectrum sampled by IRIS, a significant amount of opacity is from aerosols and/or condensates, whose spatial distribution is heterogeneous and poorly constrained, making it difficult to retrieve temperatures on isobaric surfaces at most altitudes. Three instances where this could bedone, at least approximately, is illustrated in Fig. 2, for brightness temperatures at 1304, 200 and 530 $cm^{-1}$. These brightness temperatures have been corrected to a common emission angle, using a limb function derived from observations near the equator, and they can be interpreted roughly as atmospheric temperatures averaged over thick slabs one scale height thick and centred, respectively, near 0.3 mbar in the upper stratosphere, 100 mbar, near the tropopause, and near the surface.

The 1304 $cm^{-1}$ brightness temperatures indicate the largest meridional variation, approximately 12K in the northern hemisphere between the equator and 60°. Flasar & Conrath (1990) subsequently retrieved stratospheric temperatures from the spectral radiances in the P- and Q-branches of methane at 1260-1292 $cm^{-1}$ and 1304 $cm^{-1}$, respectively (Fig. 3). These confirm the meridional contrast exhibited by the renormalised brightness temperatures and demonstrate more clearly an asymmetry of several kelvin about the equator in the upper stratosphere. Visual extrapolation suggests an equator to pole contrast of magnitude 20K, although this is highly uncertain. Recently, Coustenis et al. (1991) retrieved stratospheric temperatures from IRIS observations near 70°N and obtained 151K at 0.4 mbar, or 23K colder than the equator. An implicit assumption in all these analyses is that stratospheric methane is uniformly distributed with latitude. This is not unreasonable, given the shortness of the estimated stratospheric overturning times compared to the photochemical destruction rate, but it should be stressed that a depletion of methane at high latitudes relative to that near the equator could simulate the observed decrease of brightness temperature.

The meridional profile of the 200 $cm^{-1}$ brightness temperatures, sounding the tropopause region, is constant in two segments. Poleward of ~20°S, the brightness temperatures are 1K lower than north of ~10°S. This could be caused by an abrupt change in opacity near 10°S, implying that slightly different atmospheric levels are being sounded over the two latitude intervals, or it could result from a variation in atmospheric temperature. It is not unreasonable to anticipate the actual variation in atmospheric temperature along an isobar to be of a magnitude similar to that of the brightness temperature, but it is not really known.

The meridional variation of brightness temperature at 530 $cm^{-1}$ is nearly symmetric about the equator, decreasing ~2K from the equator to 60°; an extrapolation of 3K to the poles seems reasonable. Much of the thermal radiance in this spectral region originates at the surface (Samuelson et al., 1981; Toon et al., 1988), and Flasar et al. (1981) interpreted these variations as indicative of temperatures at the surface and in the lower troposphere. However, this interpretation has become controversial. Toon et al. (1988) have stressed that stratospheric emission also contributes a significant part of the observed 530 $cm^{-1}$ radiance. Although the opacity of the stratosphere,

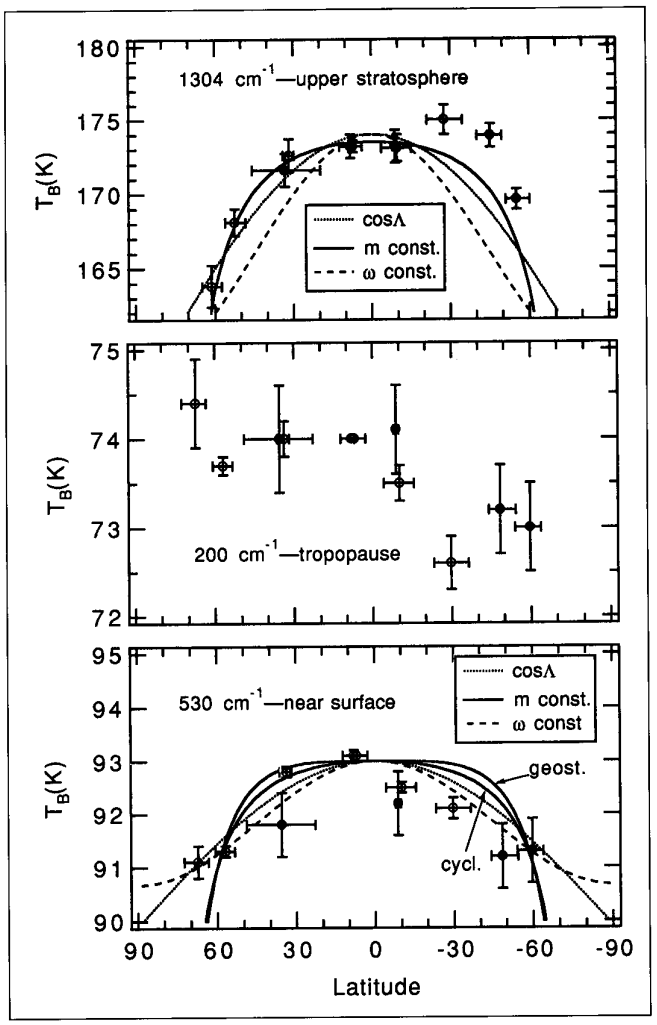


Fig. 2. Meridional distribution of brightness temperatures at 1304, 530 and 200 $cm^{-1}$. The distribution at 1304 $cm^{-1}$ is normalised to an emission angle of 47.5°, while the other two are normalised to 52.7°. Open circles are daytime data; filled circles are night-time data. The vertical bars include uncertainties from noise, calibration and emission angle corrections. The horizontal bars denote the latitude range over which the data comprising each point extends. The curve fits through the data correspond to constant angular momentum per unit mass, $m$, along isobars (solid curves); constant angular velocity, $\omega$, along isobars (dashed curves), and a temperature in which the meridional variation of temperature scales as the cosine of latitude (dotted curves). Adapted from Flasar et al. (1981).

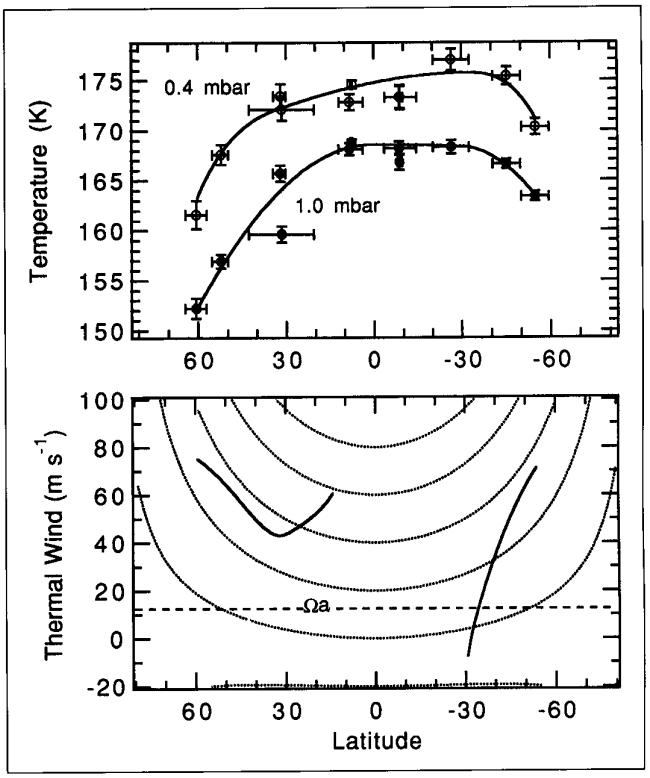


Fig. 3. *Top.* Retrieved temperature at 0.4 and 1.0 mbar. The vertical bars denote the errors attributable to instrument noise. The solid curves are smoothed fits to the temperatures. *Bottom.* Solid curves: zonal wind computed from the solid curve fitting the 1.0 mbar temperature. The thermal wind equation (3) was integrated over one scale height from an assumed state of rest. Dotted curves: loci of constant angular momentum. After Flasar & Conrath (1990).

attributable mainly to hazes, is small, the temperatures there are relatively high. The variation in surface temperatures, then, may be somewhat smaller than those of the brightness temperatures. However, the amount of the stratospheric contribution is not very well constrained.

Given the limited spatial coverage in latitude and altitude and the errors in the retrieved temperatures, application of the thermal wind equation (3) to the temperature data can provide only a rough determination of the zonal winds. Fig. 4 provides a crude analytical model of Titan's mid-latitude zonal winds based on the temperature

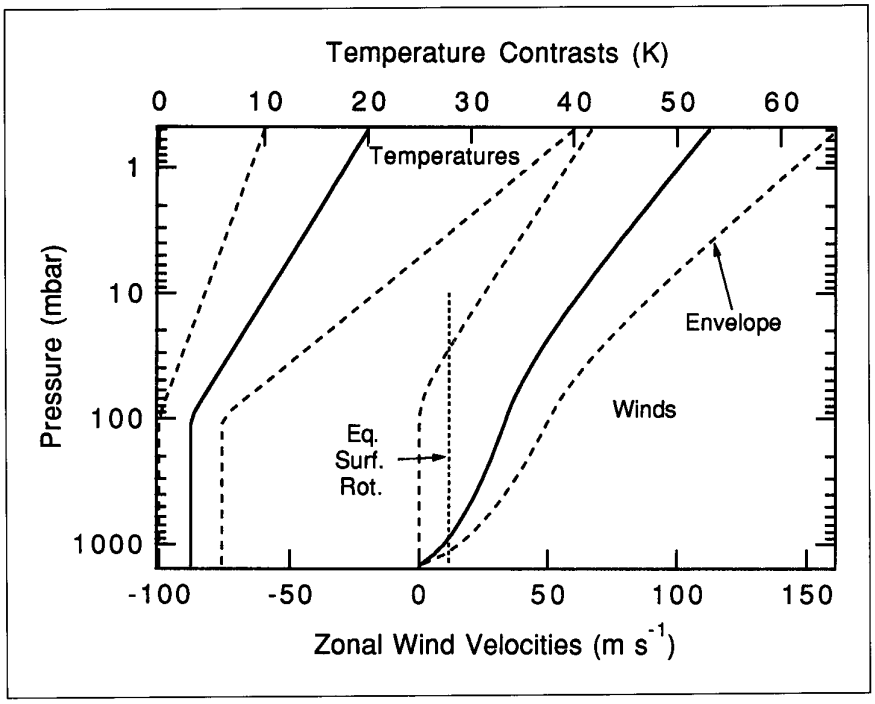


**Fig. 4. Model of vertical profile of zonal wind speed at 45° latitude, for the equator-to-pole temperature contrasts indicated. The solid curve is the nominal model, the dashed curves are a crude estimate of possible uncertainties. The larger temperature contrasts and wind speeds provide the basis for the zonal wind envelope model.**

data in Fig. 2. The solid curves denote the nominal model. The curve on the left depicts the vertical variation of the equator-to-pole temperature contrast, $\Delta T$, consistent with the temperatures in Fig. 2, assuming that the variation with latitude is given by $\Delta T \cos\Lambda$, shown as dotted curves in the top and bottom panels of Fig. 2. The curve on the right depicts the vertical profile of the zonal wind at 45° latitude implied by equation (3). In integrating equation (3), the velocity near the surface was assumed to be zero. This is consistent with measurements of zonal mean winds on Earth, and available measurements of winds on Mars and Venus, where the winds near the surface are typically small compared to those aloft because of surface drag. The dashed curves correspond to temperatures and winds for which the temperature contrasts are twice as large as the baseline model and smaller in the manner indicated. The winds in Fig. 4 are those prepared in the mid-1980s by F. M. Flasar and B. J. Conrath for the Cassini Phase A study and have been used in subsequent Huygens project planning.

The winds at low latitudes are particularly poorly determined from the temperature data because of the magnification produced by the trigonometric terms, $\tan\Lambda$ and $\sin\Lambda$, in (3), which vanish as $\Lambda \rightarrow 0$. The curves in the top and bottom panels of Fig. 2 are various fits to the meridional variation of temperature. The dotted curves depict the $\cos\Lambda$ fits just discussed. The other curves represent two limiting meridional variations in temperature that might be expected on dynamical grounds. The dashed curves assume the meridional variation of temperature scales as $\sin^2\Lambda$. If this behaviour were to characterise the vertically averaged meridional temperature variation, the implied zonal winds would correspond to uniform angular velocity: $u \propto \cos\Lambda$, and the atmospheric geopotential surfaces would correspond to simple ellipsoids with semi-major axes in the equatorial plane. The overall fit to the temperature data is not very good. As discussed earlier, the 28 Sgr results also do not support this type of behaviour in the upper stratosphere. Instead, they are more nearly consistent with the angular momentum being constant with latitude along isobars, $u \propto 1/\cos\Lambda$ in the cyclostrophic limit. This implies a vertically averaged meridional variation of temperature that scales as $\tan^2\Lambda$, which is given by the solid curve in the upper panel of Fig. 2 (Allison et al., 1994). Between 10°S and 60°N, this variation gives a reasonably good fit to the

1304 $cm^{-1}$ temperatures. Temperatures at most southern latitudes do not lie on the same curve, suggesting that the zonal winds differ in the two hemispheres. Flasar & Conrath (1990) have suggested that the temperature asymmetry is dynamical in origin, and they noted that there should be a concomitant asymmetry in angular momentum, or equivalently zonal wind, between the northern and southern hemispheres. At the northern spring season observed by Voyager 1, the winds in the southern hemisphere should have been weaker (Fig. 3). They argued that a cross-hemispheric circulation, which maintains the temperature asymmetry through adiabatic heating and cooling associated with subsidence and upwelling, respectively, is also capable of efficiently transporting angular momentum from one hemisphere to the other. Alternatively, Bézard et al. (1995) have suggested that some of the temperature asymmetry can be attributed to hemispheric differences in solar and infrared opacity sources. However, photons do not effectively transport angular momentum in planetary atmospheres, and atmospheric motions are still needed to account for the implied hemispheric asymmetry in the zonal winds. Note that the meridional gradients in temperature for all the fitted curves in the upper panel of Fig. 2 are similar at 45°, but differ significantly at high and low latitudes. This is not surprising, because the data constrain the gradients at mid latitudes best.

Similar curves are depicted in the bottom panel for the 530 $cm^{-1}$ temperatures. The constant angular momentum curves (solid) are given for both the geostrophic and cyclostrophic limits. In the former, the meridionally varying part of the temperature scales as $\sin^2\Lambda\tan^2\Lambda$. All the curves reproduce the general meridional variation of temperature, but none fits the data very well. Given the caveats mentioned earlier, this is not surprising. Again, all the curves imply similar meridional gradients at mid latitudes.

### 2.3 Theoretical studies

From a comparison of retrieved winds in Venus' atmosphere, Titan's stratospheric winds inferred from the 28 Sgr observations, and general circulation modelling (Del Genio et al., 1993), Allison et al. (1994) have pointed out a tendency for the angular momentum per unit mass to be uniform along isentropic surfaces. The numerical studies suggest that the uniformity of angular momentum is not maintained by inertial instability, which is zonally symmetric, but instead results from efficient meridional mixing of potential vorticity that acts to bring the vorticity at low and mid latitudes toward its equatorial value, which is nearly zero. They have parameterised their analysis in terms of the Richardson number, $Ri$, which, in the cyclostrophic limit, is a measure of the relative magnitude of vertical and horizontal thermal stratification. They find:

$$u(\Lambda) \leq (u(0)+\Omega r)(\cos\Lambda)^{2/Ri-1} - \Omega r\cos\Lambda \qquad (4)$$

When $Ri \rightarrow \infty$, the isentropes become horizontal and angular momentum would be uniform along isobars: $u \propto 1/\cos\Lambda$ in the cyclostrophic limit. Allison et al. note that this probably characterises the stratospheres of slowly rotating planets. Flasar & Conrath (1990) have estimated a global Richardson number of 5 in Titan's upper stratosphere; this is large enough to give a limiting velocity profile in equation (4) that is qualitatively similar to that in the $Ri \rightarrow \infty$ limit. Lower in the atmosphere, particularly near the surface, $Ri$ might be expected to be smaller. In this case, for a stably stratified atmosphere (i.e., the lapse rate in temperature is subadiabatic) in which the zonal wind increases with altitude, the isentropic surfaces will tilt, sloping upward toward the poles. The limiting zonal velocity (equation 4) increases more slowly poleward than in the $Ri \rightarrow \infty$ limit. The limiting case is for $Ri=1$, which corresponds to uniform angular velocity, and the limiting zonal velocity decreases poleward, as $\cos\Lambda$. At lower

values of $Ri$, the atmosphere is susceptible to symmetric inertial instability (Stone, 1966, 1975; Conrath et al., 1981).

### 2.4 Wind direction

In the cyclostrophic limit, centres of low pressure (equivalently, low geopotential) at the poles are consistent with zonal winds blowing in either direction (see the discussion by Flasar & Conrath 1992). Were the temperatures known to decrease poleward at all altitudes, as assumed in Fig. 4, we could infer from equation (3) that the winds would blow in the direction of Titan's rotation (here, prograde) at higher altitudes away from the surface, because the winds near the surface are small. However, the gaps in vertical coverage of both temperature and geopotential height preclude such conclusions a priori. On Venus, the one planet aside from Titan known to have a global cyclostrophic atmospheric circulation, the zonal winds blow in the direction of the planetary rotation. Theoretical considerations of the spin-up of a planetary atmosphere from a state of rest, based on Kelvin's Circulation Theorem (Flasar & Conrath, 1992), also suggest that the angular momentum associated with the planetary rotation acts as a strong constraint in maintaining the sense of this rotation as meridional circulations establish a differentially rotating atmosphere. Recent numerical experiments on the spin-up process on slowly rotating planets have yielded atmospheres that predominantly blow in the direction of the planetary rotation (Del Genio et al., 1993; Hourdin et al., 1992; Hourdin et al., 1995). Nonetheless, it is important to emphasise that dynamical systems are non-linear and often unpredictable, and presently there are no direct measurements that definitively establish the wind direction in Titan's atmosphere (however, see section 5).

### 2.5 Surface winds

Near the surface, both westerly (from the west, eastward) and easterly, winds should exist, because the net surface torque on the atmosphere should vanish. This is the case on Earth: at low altitudes, the winds at low latitudes are easterly, those at high latitudes are westerly. Drag, as noted earlier, should keep the winds small near the surface. From application of a patched Ekman-surface layer model and Rossby number similarity theory, Allison (1992) has estimated surface winds of 0.6 m/s. Flasar & Conrath (1992) have derived an upper limit to the zonally averaged wind of 0.3 m/s, by considering the axial angular momentum balance. This refers to a level at the top of the so-called 'outer' boundary layer, which is typically a few hundred metres above the surface on the Earth (Csanady, 1967; Venkatesh & Csanady, 1974).

## 3. Engineering Wind Envelope

### 3.1 Mean zonal wind

The mid-latitude wind profile in Fig. 4, corresponding to the $2 \times \Delta T$ case indicated, is the recommended vertical envelope profile of the wind speeds at 45° latitude. The variation of the winds to lower and higher latitudes is based on the limiting cases of constant angular momentum ($m$) and constant angular speed ($\omega = u/r\cos\Lambda$) on isobaric surfaces, discussed in the preceding section. In the troposphere we assume that the zonal wind speed varies as $\cos\Lambda$ along isobars at latitudes equatorward of 45° and with $m$ constant along isobars poleward of 45°, out to 60° latitude. Therefore, in the troposphere, from the surface to the tropopause (100 mbar), the envelope winds, $u$, vary with latitude as

$$u_{trop}(p,\Lambda) = \begin{cases} u(p, 45°)\sqrt{2}\cos\Lambda, & |\Lambda| \le 45° \\ \dfrac{(u(p, 45°) + \Omega r/\sqrt{2})}{\sqrt{2}\cos\Lambda} - \Omega r\cos\Lambda, & 45° < |\Lambda| \le 60° \end{cases} \quad (5a)$$

Poleward of 60°, one expects a realistic envelope of zonal velocities to deviate increasingly from constant $m$ law and decrease to zero. As Huygens will not be deployed at such high latitudes, the polar wind structure, poorly constrained by the data, is of academic interest, and we do not include it in the wind envelope model. In the upper stratosphere, the data from Voyager's IRIS near Titan's northern spring equinox and from the 28 Sgr occultation near northern summer solstice both suggest that the winds on isobaric surfaces satisfy a constant $m$ scaling from low to mid latitudes out to 60° (at least in the northern hemisphere for Voyager, the corresponding winds in the southern hemisphere were probably weaker then). Therefore we assume that at these altitudes the meridional variation of the winds on isobars is one of constant $m$ from the equator to 60°. At the 0.5 mbar level, $u$ varies as

$$u_{upstrat}(p,\Lambda) = \frac{(u(p,45°) + \Omega r/\sqrt{2})}{\sqrt{2}\cos\Lambda} - \Omega r\cos\Lambda, \qquad 0° < |\Lambda| \leq 60° \tag{5b}$$

At intermediate pressure levels, $100 < p(\text{mbar}) < 0.5$, we crudely weight (5a) and (5b) and have

$$u_{strat}(p,\Lambda) = \frac{1}{\ln 200}\left(u_{trop}\ln\left(\frac{p}{0.5\text{ mbar}}\right) + u_{upstrat}\ln\left(\frac{100\text{ mbar}}{p}\right)\right) \tag{5c}$$

At altitudes higher than the 0.5 mbar level, ≈182 km, we assume the envelope winds remain constant with altitude. Again, this is of academic interest, as Huygens' parachute will be released at a lower altitude. Fig.5 presents a meridional cross section of the wind envelope.

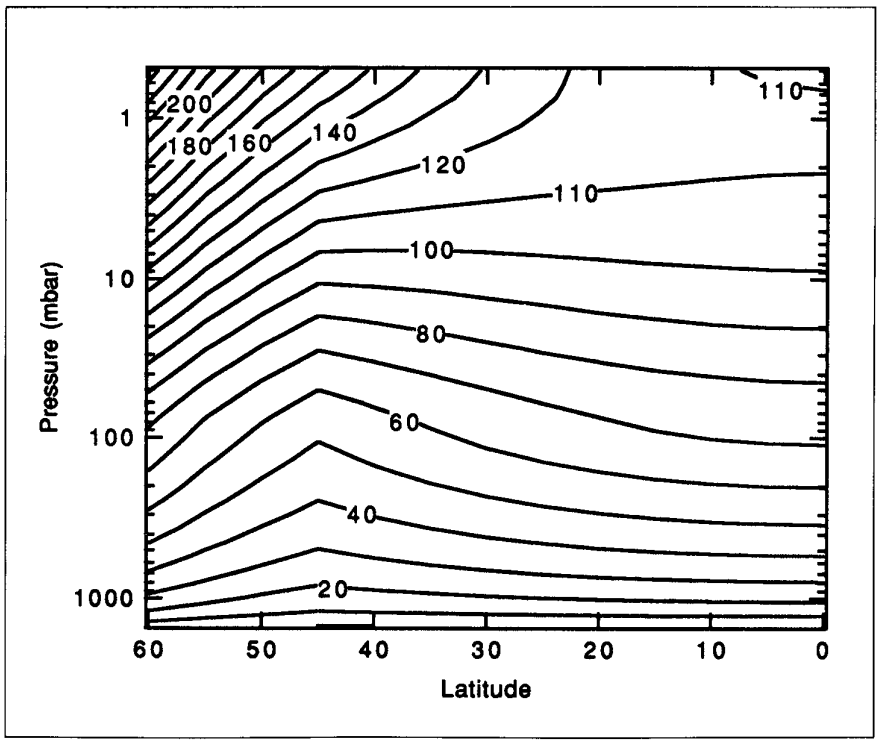


**Fig. 5. Meridional cross section of the Titan zonal wind envelope of eastward winds. The wind contours are annotated in m/s. The wind direction is uncertain, so the cross section also gives the envelope of westward winds. The envelope assumes symmetry about the equator.**

## 4. Implications for Huygens

Figure 6 depicts Huygens' lateral drift, using the wind envelope model described in the preceding section, for two simulations. The first assumes parachute deployment at 175 km altitude and a ballistic coefficient of 26.5 kg/m$^2$, resulting in a 3 h descent. The other differs in that the descent time is only 2 h. The 3 h descent profile corresponds to a linear drift of approximately 630 km. Taking into account that the wind direction is not known makes the error envelope for the Probe drift a factor of two larger. This uncertainty is currently the largest contributor to the error ellipse of the Probe's landing site.

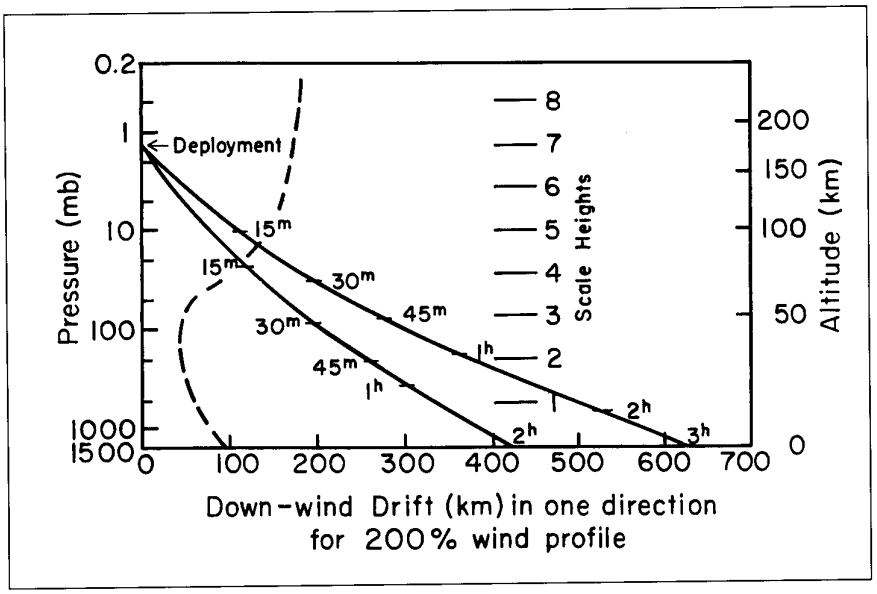


Fig. 6. Descent profiles of the Huygens probe for descent times of 2 h and 3 h.

## 5. Observations before Huygens

### 5.1 Hubble Space Telescope

Eight HST images of Titan obtained in August 1992 at near-IR wavelengths (including the methane region) with the uncorrected optics of the original Wide Field/Planetary Camera (WF/PC) clearly reveal zonal structure originating at low atmospheric levels, or possibly the surface, as reported by Smith et al. (1992, 1993). A further image sequence at 940 nm and 1080 nm was made with the refurbished Planetary Camera (WF/PC2) during 4-18 October 1994, near the time of Saturn opposition, in an attempt to detect and measure cloud-tracked winds in the lower atmosphere. Although this survey produced the first relative albedo maps of Titan's surface, cloud motions have not as yet been confidently tracked from these data (Smith et al., 1995). Hubble observations continue, however, and include further searches for discrete cloud features.

### 5.2 IR heterodyne

In August 1993, Theodor Kostiuk and collaborators (Fast et al., 1994) measured the spectrum of Titan's stratospheric ethane emission at 12 $\mu$m with the Goddard IR Heterodyne Spectrometer at NASA's IR Telescope Facility in Hawaii. The measurements were of very high spectral resolution (up to $10^{-4}$/cm) and afforded the opportunity to measure the differential Doppler shift of the emission spectra acquired on Titan's east and west limbs. This type of measurement is extremely difficult. The telescope beam size is comparable to the size of Titan's disk and centring the telescope on the limb entails significant beam dilution and a reduced signal-to-noise. The August observations used a portion of the ethane spectrum in which there were several strong lines which shifted with respect to one another as the Doppler shift changed. Several

weaker lines were also present and blended in. All this introduced uncertainties in the retrieval of the line shifts. The Doppler shifts derived indicate prograde winds in the stratosphere (1-10 mbar), with a speed ~100 m/s, but the precision of the detection is relatively low. The group will seek to confirm its findings by observing again at the IRTF, selecting spectral regions with only one or a few widely spaced lines for observation.

## References


Allison, M. (1992). A preliminary assessment of the Titan planetary boundary layer. In *Proceedings Symposium on Titan*, ESA SP-338, pp113-118.

Allison, M., Del Genio, A. D. & Zhou, W. (1994). Zero potential vorticity envelopes for the zonal-mean velocity of the Venus/Titan atmospheres. *J. Atmos. Sci.* **51,** 694-702.

Bézard, B., Coustenis, A. & McKay, C. P. (1995). Titan's stratospheric temperature asymmetry: a radiative origin? *Icarus* **113**, 267-276.

Conrath, B. J., Gierasch, P. J. & Nath, N. (1981). Stability of zonal flows on Jupiter. *Icarus* **48**, 256-282.

Coustenis, A., Bézard, B., Gautier, D., Martin, A. & Samuelson, R. (1991). Titan's atmosphere from Voyager infrared observations. III. Vertical distributions of hydrocarbons and nitriles near Titan's north pole. *Icarus* **89**, 152-167.

Csanady, G. T. (1967). On the resistance law of a turbulent Ekman layer. *J. Atmos. Sci.* **24**, 467-471.

Del Genio, A. D., Zhou, W. & Eichler, T. P. (1993). Equatorial superrotation in a slowly rotating GCM: Implications for Titan and Venus. *Icarus* **101**, 1-17.

Flasar, F. M. (1983). Oceans on Titan? *Science* **221**, 55-57.

Flasar, F. M. & Conrath, B. J. (1990). Titan's stratospheric temperatures: a case for dynamical inertia? *Icarus* **85**, 346-354.

Flasar, F. M. & Conrath, B. J. (1992). The meteorology of Titan. In *Proceedings Symposium on Titan*, ESA SP-338, pp89-99.

Flasar, F. M., Samuelson, R. E. & Conrath, B. J. (1981). Titan's atmosphere: Temperature and dynamics. *Nature* **292**, 693-698.

Fast, K. E., Kostiuk, T., Espenak, F., Buhl, D., Livengood, T. A. & Goldstein, J. (1994). Direct measurement of doppler shifts due to zonal winds on Titan. *Bull. Amer. Astron. Soc.*, **26**, 1183.

Hourdin, F. P., Le Van, P., Talagrand, O., Courtin, R., Gautier, D. & McKay, C. P. (1992). Numerical simulation of the circulation of the atmosphere of Titan. In *Proceedings Symposium on Titan*, ESA SP-338, 101-106.

Hourdin, F. P., Talagrand, O., Sadourny, R., Courtin, R., Gautier, D. & McKay, C. P. (1995). Numerical simulation of the general circulation of the atmosphere of Titan. *Icarus* **117**, 358-374.

Hubbard, W. B., Sicardy, B., Miles, R., Hollis, A. J., Forrest, R. W., Nicolson, I. K. M., Appleby, G., Beisker, W., Bittner, C., Bode, H.-J., Bruns, M., Denzau, H., Nezel, M., Riedel, E., Struckmann, H., Arlot, J. E., Roques, F., Sèvre, F., Thuillot, W., Hoffmann, M., Geyer, E. H., Buil, C., Colas, F., Lecacheux, J., Klotz, A., Thouvenot, E., Vidal, J. L., Carreira, E., Rossi, F., Blanco, C., Cristaldi, S., Nevo, Y., Reitsema, H. J., Brosch, N., Cernis, K., Zdanavicius, K., Wasserman, L. H., Hunten, D. M., Gautier, D., Lellouch, E., Yelle, R. V., Rizk, B., Flasar, F. M., Porco, C. C., Toublanc, D. & Corugedo, G. (1993). The Occultation of 28 Sgr by Titan. *Astron. Astroph.* **269**, 541-563.

Hubbard, W. B., Hunten, D. M., Reitsema, H. J., Brosch, N., Nevo, Y., Carreira, E., Rossi, F. & Wasserman, L. H. (1990). Results for Titan's atmosphere from its occultation of 28 Sagittarii. *Nature* **343**, 353-355.

Hunten, D. M., Tomasko, M. G., Flasar, F. M., Samuelson, R. E., Strobel, D. G. & Stevenson, D. G. (1984). Titan. In *Saturn* (Eds. T. Gehrels & M. S. Matthews), Univ. of Ariz. Press, Tucson, pp671-759.

Lellouch, E., Coustenis, A., Gautier, D., Raulin, F., Dubouloz, N. & Frère, C. (1989). Titan's atmosphere and hypothesized ocean: A reanalysis of the Voyager 1 radio-occultation and IRIS 7.7-mm data. *Icarus* **79**, 328-349.

Lunine, J. I., Flasar, F. M. & Allison, M. (1991). Huygens probe wind drift: science issues and recommendations. Report to the Huygens project.

Samuelson, R. E., Hanel, R. A., Kunde, V. G. & Maguire, W. C. (1981). Mean molecular weight and hydrogen abundance of Titan's atmosphere. *Nature* **292**, 688-693.

Sicardy, B., Brahic, A., Ferrari, C., Gautier, D., Lecacheux, J., Lellouch, E., Roques, F., Ariot, J. E., Colas, F., Thuillot, W., Sèvres, F., Vidal, J. L., Blanco, C., Cristaldi, S., Buil, C., Klotz, A. & Thouvenot, E. (1990). Probing Titan's atmosphere by stellar occultation. *Nature* **343**, 350-353.

Smith, B. A., Soderblom, L., Beebe, R., Boyce, J., Briggs, G., Bunker, A., Collins, S. A., Hansen, C. J., Johnson, T. V., Mitchell, J. L., Terrile, R. J., Carr, M., Cook II, A. F., Cuzzi, J., Pollack, J. B., Danielson, G. E., Ingersoll, A., Davies, M. E., Hunt, G. E., Masursky, H., Shoemaker, E., Morrison, D., Owen, T., Sagan, C., Veverka, J., Strom, R. & Suomi, V. E. (1981a). Encounter with Saturn: Voyager 1 imaging science results. *Science* **212**, 163-191.

Smith. B. A., Soderblom, L., Batson, R., Bridges, P., Inge, J., Masursky, H., Shoemaker, E., Beebe, R., Boyce, J., Briggs, G., Bunker, A., Collins, S. A., Hansen, C. J., Johnson, T. V., Mitchell, J. L., Terrile, R. J., Cook II, A. F., Cuzzi, J., Pollack, J. B., Danielson, G. E., Ingersoll, A., Davies, M. E., Hunt, G. E., Morrison, D., Owen, T., Sagan, C., Veverka, J., Strom, R. & Suomi, V. E. (1981b). A new look at the Saturn system: The Voyager 2 images. *Science* **215**, 504-537.

Smith, P. H., Karkoschka, E. & Lemmon, M. (1992). Titan's north-south asymmetry from HST images. *Bull. Am. Astron. Soc.* **24**, 950.

Smith, P. H. & Lemmon, M. (1993). HST images of Titan. *Bull. Am. Astron. Soc.* **25**, 1105.

Smith, P. H., Lemmon, M. T., Lorenz, R. D., Sromovsky, L. A., Caldwell, J. J. & Allison, M. D. (1996). Titan's surface, revealed by HST imaging. *Icarus* **119**, 335-349.

Stone, P. H. (1966). On nongeostrophic baroclinic instability. *J. Atmos. Sci.* **23**, 390-400.

Stone, P. H. (1975). The meteorology of the Jovian atmosphere. In *Jupiter* (Ed. T. Gehrels), Univ. Ariz. Press, pp586-718.

Toon, O. B., McKay, C. P., Courtin, R. & Ackerman, T. P. (1988). Methane rain on Titan. *Icarus* **75**, 255-284.

Venkatesh, S. & Csanady, G. T. (1974). A baroclinic planetary boundary layer model, and its application to the Wangara data. *Bound.-Layer Met.* **5**, 459-473.